Bioconjugate Chemistry

Article

pubs.acs.org/bc

XAV939: From a Small Inhibitor to a Potent Drug Bioconjugate When Delivered by Gold Nanoparticles

Marwa M. Afifi, Lauren A. Austin, Megan A. Mackey, and Mostafa A. El-Sayed*

Laser Dynamic Laboratory, School of Chemistry and Biochemistry, Georgia Institute of Technology, Atlanta, Georgia 30332-0400,United States

Supporting Information

ABSTRACT: Nanoparticles as potential drug delivery vectors are drawing more attention every day. Here, we used gold nanopspheres (AuNSs) to selectively target the Wnt signaling pathway in human oral squamous cell carcinoma (HSC-3) cells. In a previously conducted study, XAV939, a small inhibiter, was found to strongly regulate the Wnt pathway by inhibiting the tankyrase enzyme and subsequent stabilization of cytoplasmic axin levels. In the present study, conjugating XAV939 molecules to AuNSs is found to enhance its potency by at least 100 times over its free form in killing HSC-3 cancer cells. Additionally, XAV 939 uptake studies have demonstrated an enhanced XAV939 bioconjugate delivery to the targeted cells compared to the passive cellular diffusion of the free drug at the same concentration. Furthermore, our study revealed that drug delivery and cytotoxicity are directly related to the size of the functionalized nanoparticles.

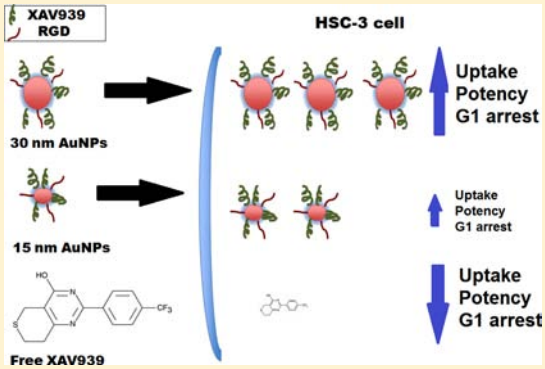

INTRODUCTION

In the past decade, nanoparticles (NPs), specifically gold nanoparticles (AuNPs), were found to have significant applications in the field of biology and medicine.[1−7] AuNPs have unique physical and chemical properties such as their lack of inherent cytotoxicity, biological stability, facile synthesis, and their ability to easily bind to a wide range of biomaterials such as peptides, enzymes, DNA, genes, and drugs.[2,8] These characteristics make them excellent candidates for bioconjugation with different moieties.[9,10] The ability to tune the surface biochemistry of the AuNPs by loading specific ligands enables their potential application in disease therapy (e.g., drug carriers) and diagnostic devices.[11] Furthermore, several groups have demonstrated the ability of AuNPs to improve the solubility, stability, and efficacy of chemotherapeutic drugs, thereby enhancing their potency while minimizing adverse toxic effects.[12,13]

Functionalizing AuNPs with selective targeting ligands has been recently documented.[9,11,12,14−18] Gong and co-workers reported using doxorubicin functionalized AuNPs as pH-responsive anticancer drug carriers.[9] El-Sayed and co-workers have shown that tamoxifin functionalized AuNPs selectively target estrogen receptor alpha in human breast cancer cells with up to 2.7 times enhanced potency compared to the free drug form *in vitro*.[12] Additionally, Huang et al. demonstrated that oral cancer cells expressing human epidermal growth factor receptor (EGFR) can be selectively targeted and photothermally destroyed by gold nanospheres and nanorods targeted with IgG antibodies *in vitro*.[19]

Wnt proteins (Wnts) are a family of 19 glycosylated and lipidated proteins that regulate cell growth and differentiation. These proteins are the driving regulator during embryogenesis, as they control cellular morphogenesis and organ differentiation.[20] In adult cells, Wnts maintain the self-renewal process of tissues such as mucosa, skin, bone marrow, and gut.[21] They elicit their effect by binding to Wnt cell receptors, sparking intracellular transduction signals mediated by β-catenin which translocates into the nucleus, transcribing nuclear target genes.[22] The Wnt signaling pathway is regulated by the controlled degradation of β-catenin in the cytoplasm. In dormant cells, β-catenin cellular levels are kept low by the intracytoplasmic β-catenin degradation complex (axin, adenomatous polyposis coli (APC) and glycogen synthase kinase (GSK-3β)).[23] Deregulation of the Wnt signaling pathway and the consequent accumulation of the intracellular β-catenin have been implicated as a driver of osteoporosis, degenerative disorders, and several types of cancer including oral cancer.[24−27] The tankyrase enzyme has been implicated in Wnt/β-catenin signaling by labeling axin, causing its degradation, and subsequently stabilizing the cellular pooling of β-catenin. Recently, tankyrase has been recognized as a potential target for anticancer drugs.[28,29] In 2009, Huang et al.[28] identified a small molecule inhibitor of the Wnt/β-catenin pathway named XAV939, which selectively inhibits β-catenin mediated transcription. XAV939 stimulates β-catenin degrada-

Received: June 8, 2013
Revised: December 9, 2013
Published: December 11, 2013

tion by stabilizing the intracellular axin level, which is the concentration-limiting component of the destruction complex.[28] Due to the link between the Wnt signaling pathway and oral cancer,[25,30,31] we chose to functionalize gold nanospheres (AuNSs) with XAV939 to act as a nuclear targeting ligand against human oral squamous cell carcinoma (HSC-3) cells. We further investigated the functionalization of XAV939 on AuNSs of two different sizes (15 and 30 nm) in terms of cellular uptake, potency, and efficacy when compared to the free form of XAV939.

EXPERIMENTAL SECTION

Preparation of Gold Nanospheres (AuNSs). AuNSs were prepared by the sodium citrate reduction method.[32] Briefly, for 30-nm-sized AuNS, 50 mL of 0.01% (by weight) $HAuCl_4$ (Sigma-Aldrich) aqueous solution was heated to boiling while stirring in a 100 mL beaker. Next, 1 mL of a 1% (by weight) trisodium citrate (Sigma-Aldrich) aqueous solution was added. The same method was used to prepare the 15 nm AuNS, but the sodium citrate concentration was increased to 2%.[32] In both syntheses, solution changed in color from yellow to black and then red indicating nanoparticle formation.

AuNSs Bioconjugation with Peptides and XAV939. For both nanoparticle sizes, the same conjugation process was executed and the same amount of drug percent coverage was attained for both 15 and 30 nm AuNSs.

Poly(ethylene glycol) (PEG) polymer was used to stabilize the nanoparticles to inhibit their aggregation during the drug–peptide conjugation.[33] A 1.0 mM solution of m PEG-SH (MW 5000, Laysan Bio, Inc.) dissolved in deionized water (DI water) was added to the nanoparticles solution to achieve a mole ratio equivalent to 25% of gold nanoparticle's surface (ca. 710 PEG ligands were added per particle). The PEG-stabilized AuNSs solution was allowed to shake at room temperature for 24 h, after which excess PEG was removed by centrifugation (6000 rpm, 14 min). The washed PEG-AuNSs (P-AuNSs) were redispersed in DI water. The achieved Au-SR bond had a bonding affinity of ca. 40 kcal mol^{-1}.[34]

The RGD peptide is known to target $\alpha_v\beta_6$ surface integrins, expressed on HSC-3 cells, increasing nanoparticle uptake by the cancer cells.[35,36] A custom RGD peptide (RGDRGDRGDRGDPGC) purchased from GenScript USA, Inc. was used to further functionalize the particles. A 5.0 mM RGD solution dissolved in DI water was added to the nanoparticle solution to achieve a mole ratio equivalent to 15% surface coverage (ca. 430 RGD ligands were added per particle). The PEG-RGD-AuNS solution was left to shake for 24 h at room temperature and excess peptides were removed by centrifugation (6000 rpm, 14 min). The PEG-RGD AuNSs (PR-AuNSs) were redispersed in DI water. The final established Au-NH2R bond had a strength value of ca. 8 kcal mol^{-1}.[37]

Finally, XAV939 was conjugated to the PEG-RGD-AuNSs. The drug was loaded to the gold nanoparticles via a sulfide linkage to establish a high binding affinity (ca. 20 kcal mol^{-1}).[38] A 6.4 mM solution of XAV939 in DMSO (Cayman Chemicals, USA) was added to the PEG-RGD-AuNSs to accomplish a mole ratio equivalent to 65% surface coverage (ca. 1850 XAV ligands per particle). The solution was allowed to react for 24 h at room temperature, after which the excess drug was removed by centrifugation (6000 rpm, 14 min). The conjugation process is schematically shown in Figure 1. Throughout the study, PEG-RGD-XAV AuNSs will be referred as PRX-AuNSs.

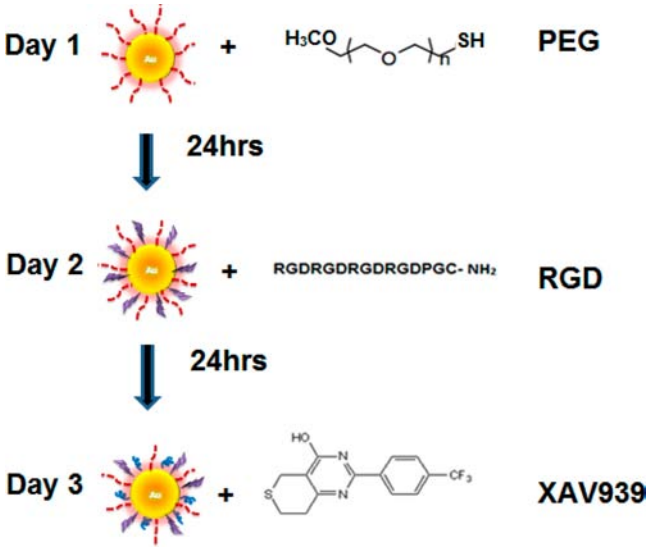

Figure 1. Schematic diagram for the synthesis of XAV939 bioconjugated AuNPs.

Characterization of Bioconjugated AuNSs. The conjugated AuNSs were characterized using UV–vis spectroscopy (OceanOptics, HR4000CG- UVNIR, USA) and transmission electron microscopy (TEM, JEOL, 100CXII, Redding, CA, USA). Zeta potential of the AuNSs and conjugates was measured using a NanoZS Zetasizer particle analyzer (Malvern, USA) equipped with a 633 nm laser.

Drug Encapsulation Efficiency. Equal volume of dichloromethane (DCM) and aqueous solutions of PRX-AuNSs were slowly added to a 1 cm quartz cuvette and the mixture was kept at room temperature. The absorption spectrum for the XAV939 in DCM was measured every 30 min for 4 h. XAV939 absorbance peak (313 nm) was not seen over the 4 h period of time, suggesting that the drug is directly conjugated to the particle via a strong covalent bond.[39,40]

Cell Cultures and Nanoparticle/Drug Treatments. HSC-3 (human oral squamous cell carcinoma), a malignant epithelial cell line expressing $\alpha_v\beta_6$ integrins on the cell membrane, was chosen as our cancer cell model.[41] HaCaT (spontaneously immortalized human keratinocytes), a non-malignant epithelial cell line, was used as the healthy control cell line. Both cell lines were cultured in Dulbecco's Modified Eagle's Complete Medium (DMEM) (Mediatech) supplemented with 4.5 g/L glucose and sodium pyruvate, 10% v/v fetal bovine serum (FBS) (Mediatech), and 1% antimycotic solution (Mediatech). Cell cultures were kept at 37 °C in a 5% CO_2 humidified incubator. The XAV-conjugated AuNSs were dispersed in complete DMEM to the final required ligand (XAV939) concentration. The previously determined extinction coefficients, (3.6×10^8 and 3×10^9 L mol^{-1} $cm^{-1}$for the 15 and 30 nm AuNSs, respectively) were used to calculate the final concentrations of the prepared PRX-AuNSs solutions. As controls, both cell lines were incubated with an equivalent concentration of the free XAV939 for the same period of time. When comparing the free and bioconjugated forms of the drug, both were reported as the effective concentration of the drug bound to the nanoparticles.

dx.doi.org/10.1021/bc400271x | Bioconjugate Chem. 2014, 25, 207–215

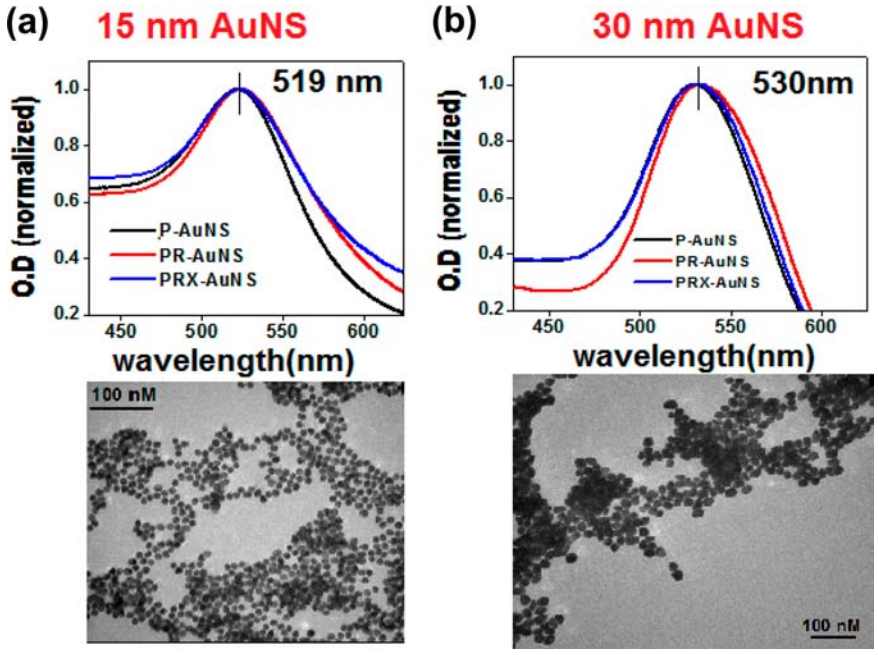

Figure 2. Structural and optical properties of synthesized AuNS. TEM images and optical absorption spectra showing an average size of 15 nm (a) and 30 nm (b) gold nanospheres. UV−vis measurements showed minimal shift in the spectrum of the AuNPs after conjugation with PEG, RGD, and XAV939 indicating stability and minimal increase in the particle size.

Cell Viability Assays and Cellular Cytotoxicity. *In vitro* cytotoxicity of XAV939 bioconjugates versus free XAV939 was assessed against HSC-3 and HaCaT cells using a XTT cell viability assay (Biotium, Hayward, CA, USA). The pale yellow XTT reagent (2,3-bis-(2-methoxy-4-nitro-5-sulfophenyl)-2*H*-tetrazolium-5-carboxanilide) changes to the bright orange formazan product by mitochondrial enzymes in viable cells. Cells were split at 70% confluence in a 96-well plate and incubated for 24 h at 37 °C in a 5% CO_2 humidified atmosphere. Culture medium was removed and replaced with complete DMEM containing different concentrations of XAV939 and reincubated for 48 and 96 h. Control wells were incubated with fresh culture media. The assay was analyzed using a Biotek Synergy H4Multi-Mode Plate Reader following the manufacturer's instructions.

Regression analysis was used to model the relationship between cellular viability and XAV939 concentration (μM). The effective concentration of the drug required for 50% cellular death was denoted by EC50. Drug−dose response curves for the bioconjugated and free XAV939 were generated (normalized to DMSO). Regression analysis was used to determine the 95% confidence limits for the predicted drug EC50 for both free and bioconjugated drug cytotoxicity respectively. Statistical analysis was done using ANOVA test. Data was considered statistically significant if the P value was <0.05.

Cell Cycle Analysis Using Flow Cytometry. Cells were grown for 24 h in complete DMEM and then incubated with free and conjugated XAV939 dissolved in fresh DMEM for 48 h, after which cells were harvested using trypsin, washed with phosphate buffered saline (PBS), fixed in ice-cold ethanol (70%), and kept at −20°C. Fixed cell suspensions were centrifuged at 1500 rpm for 7 min and the cell pellet was redispersed in PBS. Cells were treated with 200 μg/mL RNase (Sigma) for 30 min at 37°C. Following this, DNA staining with 100 μg/mL of propidium iodine (Sigma) was performed at room temperature for 15 min. A BD LSR II flow cytometer (BD Biosciences) with 488 nm excitation laser and fluorescence detection in the PE channel was used to measure the cell cycle distribution (15 000 events were acquired for each sample). The obtained data was analyzed using FloJo (Tree Star Inc.), a flow cytometry analyzing software. The amount of propidium iodide intercalated to DNA was used as a parameter to determine the cell cycle distribution phases.

AuNSs Cellular Internalization and Drug Uptake. HSC-3 and HaCaT cells were cultured on 18-mm-diameter glass coverslips and incubated for 24 h at 37°C. Afterward, the culture medium was removed and replaced with 0.5 nM PRX-AuNSs solutions prepared in complete DMEM. Control wells were treated with PR-AuNSs at the same concentration. The cells were incubated for another 24 h. The coverslips were then washed with DPBS buffer. A previously developed etching protocol was used to remove any AuNSs on the outer surface of the cell membrane.[42] Briefly, 1 mL of an aqueous solution of 1:6 molar ratio of I_2 (0.34 mM) and KI was added to the cells for 5 min. The coverslips were then washed with DI water and fixed with 4% paraformaldehyde. Images were obtained with an inverted Olympus IX70 microscope with a dark field condenser (U-DCW). A 100×/1.35 oil Iris objective (UPLANAPO) was used to collect the scattered light from the AuNSs treated samples.

HSC-3 and HaCaT cells were incubated for 24 h in complete red DMEM, after which the culture media was replaced with 0.5 nM of XAV-conjugated AuNSs solutions diluted in DMEM for an additional 48 h. AuNSs solutions were removed and the solution's absorbance values at the adopted maximum extinctions were taken using a microplate reader (Biotek Synergy H4Multi-Mode Plate Reader). Cells were counted using an inverted Olympus IX70 microscope with a 10× objective. Ligand uptake values were normalized to the number of cells and were reported as number of ligands. Statistical significance ($P < 0.05$) was determined from the comparison of

dx.doi.org/10.1021/bc400271x | *Bioconjugate Chem.* 2014, 25, 207−215

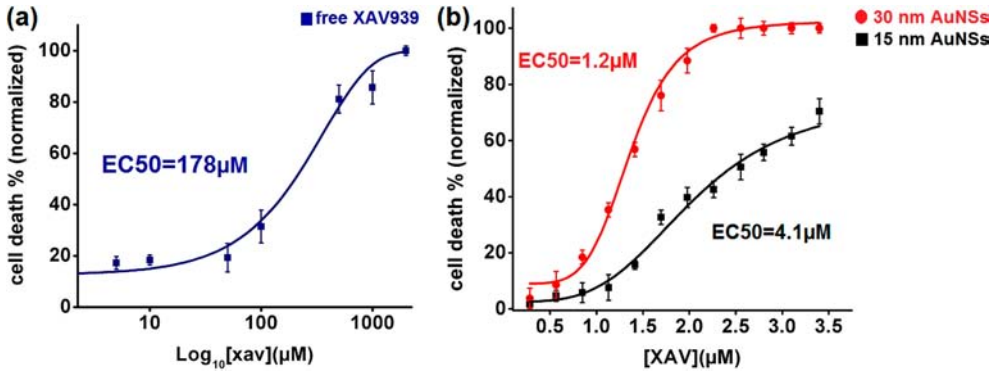

Figure 3. Dose-dependent curves for cellular cytotoxicity of HSC-3 cells incubated with free (a) and ligated XAV939 to 15 and 30 nm AuNSs for 96 h (b). EC50 values for the free and bioconjugated XAV939 were 178, 4.1, and 1.2 μM, respectively. The conjugated form exhibits 2 orders of magnitude increased potency when compared to the free drug ($P < 0.05$).

cancer (HSC-3) treated cells and healthy (HaCaT) treated cells.

Statistical Analysis. Statistical analysis for experimental values was carried out as mean ± standard deviation of triplicate experiments. The data, except the cytotoxicity results, were analyzed using the *t* test calculator (GraphPad Software, GraphPad Software, Inc.). Statistical significance was determined from untreated (control) to treated (XAV939 bioconjugates and free drug incubation) samples. Statistical analysis was also performed between samples treated with XAV939 bioconjugated to 15 and 30 nm AuNSs. Data was considered statistically significant if the *P* value was <0.05.

RESULTS AND DISCUSSION

Characterization of the AuNSs and Bioconjugates. AuNSs of 15 and 30 nm diameters were synthesized using the citrate reduction method. For both nanoparticle sizes, the same conjugation process was executed and the same amount of drug percent coverage was attained for both-sized particles. AuNSs were first stabilized by a thiol linked PEG. This was followed by adding RGD peptides, which target HSC-3 cellular surface integrins. Finally, XAV939 inhibitor was conjugated to both sizes of AuNSs (Figure 1). They were characterized using TEM and UV−vis spectroscopy, which confirmed the desired shape, size, and conjugation process (Figure 2).

After conjugating the AuNSs with PEG, RGD, and XAV939, there was no significant change in the UV−vis spectra between P-AuNSs, PR-AuNSs, and PRX-AuNSs. This indicates the formation of stable, monodispersed nanospheres. Furthermore, the minimal shift in the spectra can be associated with the change in AuNSs surface modifications, yet suggests a negligible increase in the nanoparticles size after conjugation. The zeta potential values for P-AuNSs, PR-AuNSs, and PRX-AuNSs were −9.54, −6.23, and −2.6 mV, respectively, confirming successful drug conjugation.

Cytotoxicity Studies for HSC-3 Cells after XAV939-AuNSs Treatment. To investigate the effect of XAV939 bioconjugation to different-sized AuNSs in term of enhancing the XAV939 potency, cytotoxicity assays were conducted. We first compared the drug functionalized nanoparticles (15 and 30 nm) to the free form at treatment times of 48 and 96 h. Figures 3 and S1 show the drug−dose response curves for the free (Figures 3a, S1a) and bioconjugated XAV939 (15 and 30 nm) (Figures 3b, S1b) after being incubated with the HSC-3 cells for 48 and 96 h. The EC50 values for the free and bioconjugated XAV939 15 and 30 nm AuNSs were found to be ∼2 mM, 4.8 and 2.7 μM (Figure S1), respectively, after 48 h. Increasing the treatment time to 96 h decreased the EC50 values to 178, 4.1, and 1.2 μM (Figure 3), respectively. This suggests the following: XAV939 has a slow mode of action, and functionalization with the nanoparticles increased the drug's cytotoxic potency by more than 100 times that of the free form at both time points ($P < 0.05$). The increased potency of the bioconjugates is attributed to the AuNSs receptor mediated cellular endocytosis versus passive diffusion of the free drug into the cell. Within this context, we chose to compare the cytotoxicity of XAV939 against HSC-3 cells and other widely documented anticancer drugs (Table 1). The free form of XAV939 inhibitor showed an EC50 value of 2 mM, 178 μM against HSC-3 cells after an incubating period of 48 and 96 h, respectively. In the world of anticancer drugs, this value seems relatively high. On the other hand, loading the small inhibiter XAV939 to AuNSs boosted its cytotoxic affect to compete with some of the popular anticancer drugs (Table 1).

Table 1. Comparison between the EC50 of XAV939 and Some Popular Anticancer Drugs/Inhibiter against HSC-3 Cells

drug/inhibiter	EC50 (μM)
XAV939 bioconjugates	1.2 μM
Free XAV939	178 μM
Cisplatin[56]	16 μM
5-Fluorouracil [56]	89 μM
Doxorubicin[57]	3.55 μM
Tamoxifin[58]	13 μM

We additionally studied the effect of the nanoparticle size on enhancing the drug potency against the HSC-3 cells. Figure 4 shows the HSC-3 cell viability when treated with 15 and 30 nm XAV939 conjugated AuNS after 48 and 96 h. Incubating HSC-3 cells with 15 and 30 nm PRX-AuNSs at 0.1, 0.5, and 1 nM for 48 h showed a concentration-dependent decrease in cell viability. Specifically, as shown in Figure 4a, 30 nm PRX-AuNSs induced more HSC-3 cell death (ca. 40%) compared to the smaller functionalized nanoparticles (ca. 10%) at the same concentration after 48 h treatment ($P < 0.05$). Increasing the time of incubation to 96 h showed a significant increase in HSC-3 cell death treated with the larger bioconjugated nanoparticles (ca. 80%), while no significant change was seen in the case of the smaller AuNSs (ca. 10%). Accordingly, enhancing the XAV939 bioconjugate cytotoxicity against cancer

dx.doi.org/10.1021/bc400271x | *Bioconjugate Chem.* 2014, 25, 207−215

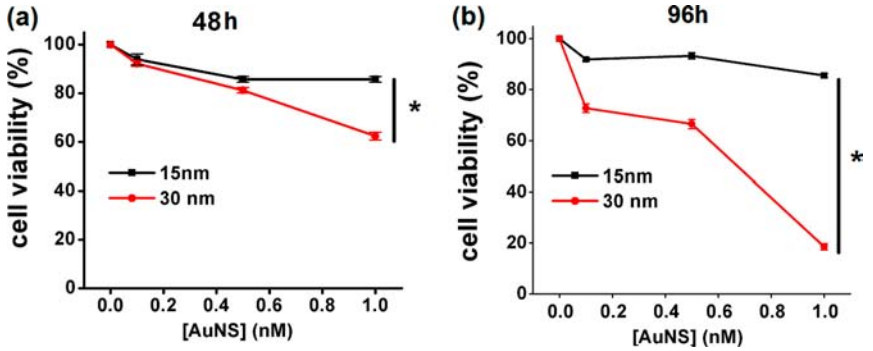

Figure 4. Drug-dose-dependent curve showing the nanoparticle size effect on enhancing the XAV939 cytotoxic effect against HSC-3 cells at 48 (a) and 96 (b) h time intervals. (a) After 48 h of cell incubation with drug-functionalized particles, 30 nm PRX-AuNSs showed significantly higher cytotoxicity compared to 15 nm PRX-AuNSs at all concentrations ($P < 0.05$). (b) HSC-3 cells incubated with 30 nm PRX-AuNSs for 96 h showed marked decrease in cell viability 20%; 90% cell viability in the case of cancer cells treated with 15 nm PRX-AuNS at the same concentrations. Graphs (a) and (b) reveal functionalized 30 nm AuNSs showing higher HSC-3 cytotoxicity at all concentrations than the 5 nm nanoparticles. Moreover, increasing the incubation time showed increased HSC-3 death treated with 30 nm AuNSs, while no significant change was noticed in case of cells incubated with the 15 nm AuNSs. All data were normalized to DMSO %. Data is represented as mean ± SD of three independent experiments. Statistical significance is denoted by an asterisk ($P < 0.05$).

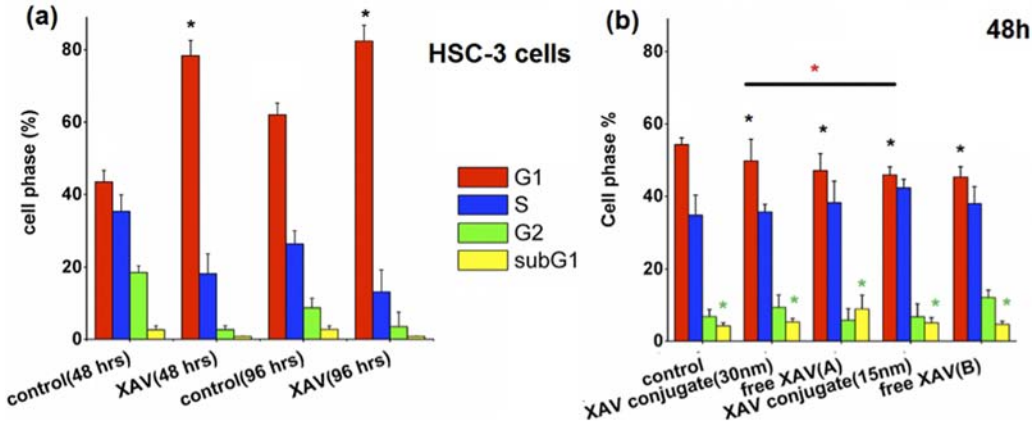

Figure 5. Cell cycle analysis of HSC-3 cells after incubation with 50 μM XAV939 (a) and XAV939 functionalized 15 and 30 nm AuNSs and equivalent concentration of the free form, 0.2 and 0.9 μM (b). (a) Incubating HSC-3 cells with 50 μM XAV939 showed a significant increase ($P < 0.05$) in G1 arrest, in correlation with time. (b) HSC-3 cells exhibited a significantly higher % of G1 (black asterisk) and subG1 (green asterisk) arrest after 48 h incubation with XAV939 bioconjugates (30 and 15 nm AuNSs) compared to the free drug version (A and B), respectively ($P < 0.05$). Furthermore, larger sized nanoparticles loaded with XAV939 showed significantly higher % of G1 arrest compared to small-sized ones (red asterisk, $P < 0.05$). Data is represented as mean ± SD of three independent experiments. Statistical significance is denoted by an asterisk ($P < 0.05$).

cells is significantly correlated to the nanoparticle size ($P < 0.05$). The larger sized XAV939 conjugated-AuNSs showed lower viability in HSC-3 cells compared to the smaller AuNSs at the same concentration and incubation period. As stated previously, both the bioconjugated and free forms of XAV939 showed a relatively slow mode of action. Functionalizing the 30 nm AuNSs with XAV939 dramatically decreased the effective drug concentration but did not accelerate the time of exposure required for such effect.

To exclude any cytotoxic effect of other surface ligands on different sized AuNSs, HSC-3 cells were treated with PEG and RGD functionalized AuNSs. Cell viability assay results showed no to minimal cell death associated with non-XAV939 AuNSs (Figure S3).

Cell Cycle Analysis of Free and Bioconjugated XAV939 Treated HSC-3 Cells. To further assess the mechanism behind these observed cytotoxicites, we examined the cell cycle distribution after treatment of HSC-3 cells with bioconjugated and free XAV939 for 48 and 96 h. We also investigated if the cell cycle distribution is dependent on the size of the drug functionalized nanoparticles.

Based on cell viability results, both cell lines were treated with 50 μM free XAV939 for 48 and 96 h. As shown in Figure 5a, incubating HSC-3 cells with 50 μM XAV939 for 48 and 96 h showed a significant increase in the G1 phase compared to the untreated cells (controls) at the same time intervals. Faulty G1 cell phase control has been linked to oncogenes, tumor suppressor genes, and therapeutic agents targeting them. For any cell to enter the S-phase and participate in subsequent DNA replication, Cyclin-Dependent Kinases (CDKs) must first be activated via binding to cyclin proteins. Several researchers have outlined different signaling pathways, including Wnt/β, which controls cyclin concentrations, authorizing CDKs to constrain the G1/S transition. That is to say, the Wnt/β pathway acts as a downstream regulator for cellular proliferation in the G1 phase. Therefore, when XAV939 targets and inhibits the tankyrase enzyme, subsequent axin level stabilization and β catenin degradation will ultimately occur resulting in G1 arrest.[43,44]

dx.doi.org/10.1021/bc400271x | *Bioconjugate Chem.* 2014, 25, 207−215

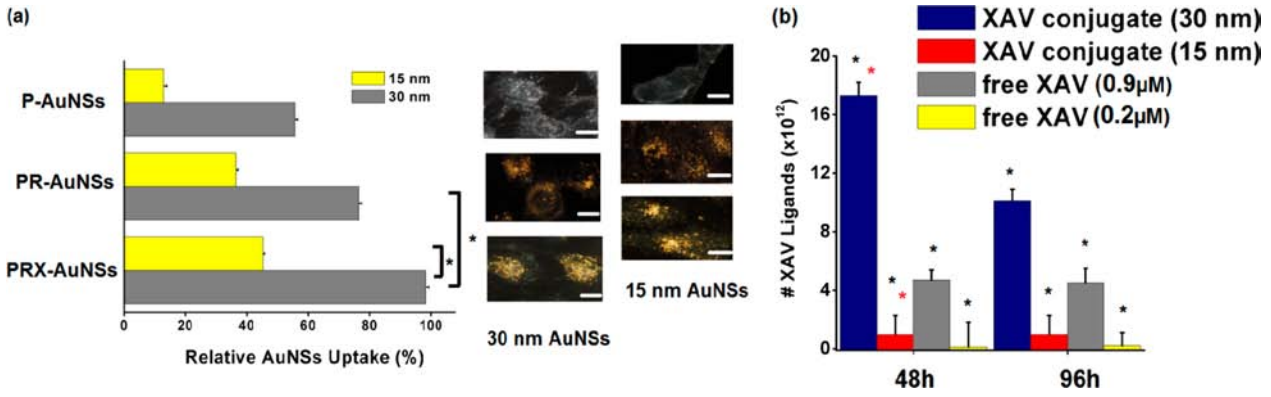

Figure 6. (a) Dark field images for HSC-3 cells incubated with 0.5 nM of 30 (gray) and 15 (yellow) nm and PRX-AuNSs, PR-AuNSs, and P-AuNSs. HSC-3 cells showed successful nuclear localization of both 15 and 30 nm PRX-AuNSs after 24 h incubation. Both sizes of P-AuNSs showed no cellular internalization, while PR-AuNSs cellular uptake was fairly lower than PRX particles ($p < 0.05$). (b) Quantification of the number of bioconjugated XAX939 loaded on 30 (blue) and 15 (red) nm AuNSs internalized by HSC-3 cells compared to free XAV939 at the same concentration as that ligated XAV939 to 30(A) and 15(B) nm AuNSs (gray and yellow), respectively, at 48 and 96 h. As shown, 30 and 15 nm drug functionalized nanoparticles transport significantly more XAV939 ligands to the HSC-3 cells than the free form ($P < 0.05$, black asterisk) at both time points. Moreover, XAV939 functionalized 30 nm nanoparticles delivered an order of magnitude higher drug ligands than 15 nm ones ($P < 0.05$, red asterisk). Data is represented as mean ± SD of three independent experiments. Statistical significance is denoted by an asterisk ($P < 0.05$). Scale bar: 10 μm.

Next, we compared HSC-3 cell changes when treated with the drug functionalized AuNSs (15 and 30 nm) and those incubated with the free drug at the same concentrations (ca. 0.2 and 0.9 μM, respectively) and time points. After 48 h incubation, the HSC-3 cells treated with XAV939 functionalized AuNSs showed significantly higher G1 arrest than both controls and cells treated with the free drug at the same concentration, $P < 0.05$ (Figure 5b). Furthermore, G1 arrest caused by bioconjugated XAV939 was found to be dependent on the size of AuNSs, where 30 nm nanoparticles exhibited significantly higher percentage of G1 arrest than those of 15 nm (Figure 5b, $P < 0.05$). It is worth mentioning that HSC-3 cells incubated with PEG and PEG-RGD AuNSs did not show cell cycle changes when compared to XAV939 bioconjugates (Figure S4).

XAV939 Bioconjugate Localization and Drug Uptake in HSC-3 cells. In order to further explain the cell cycle changes and the associated cell cytotoxicity results, we looked at the XAV939 cellular localization and uptake by the HSC-3 cells. The intracellular internalization of the drug loaded 15 and 30 nm nanoparticles was assessed using dark field imaging via the light scattering property of the AuNSs.[45] Figure 6a shows representative images of HSC-3 cells treated with 0.4 nM PRX-AuNSs, PR-AuNSs, and P-AuNSs for 24 h. HSC-3 cells showed a high degree of intracellular and perinuclear accumulation of PRX-AuNS. The conjugation of XAV939 drug molecules and RGD peptides allowed the AuNSs to actively target and interact with the HSC-3 cells resulting in more intracellular localization when compared to P-AuNSs alone.[28,33,46] On the other hand, the intracellular accumulation of PR-AuNSs within HSC-3 cells was fairly less than that of PRX-AuNSs ($p < 0.05$), implying that XAV939 molecules do have a role in cellular endocytosis.

The relative uptake of the free and conjugated XAV939 was quantified in the HSC-3 cells after 48 and 96 h of treatment. Figure 6b shows the HSC-3 cellular uptake of the drug bioconjugated to 15 and 30 nm AuNSs compared to the free form at the same concentration (ca. 0.2 and 0.9 μM, respectively) after 48 h treatment. As shown in Figure 6b, the number of XAV bioconjugates (15 and 30 nm AuNSs) taken up by the HSC-3 cells was significantly higher than that of the free drug ($P < 0.05$), when compared at 48 and 96 h time points. By comparing the HSC-3 cellular uptake values for XAV939 bioconjugates at both time intervals, we noticed that the 30 nm functionalized AuNSs showed greater uptake after 48 h than 96 h. As for the 15 nm conjugated AuNSs, there was an equal amount of drug bioconjugate uptake for 48 and 96 h treatments (Figure 6b).

Additionally, we determined the effect of the drug-loaded AuNS size on the HSC-3 cellular uptake. At a given optical density value, the number of 15 nm AuNSs was found to be greater than the 30 nm AuNSs. Subsequently, the number of XAV939 molecules will be higher in the case of the small-sized conjugated AuNSs (at the same surface coverage %). Nevertheless, when we used the same concentration for both sizes of AuNSs, the larger surface area of the 30 nm AuNSs allows for better drug loading capacity per one particle. Figure 6b illustrates that the number of XAV939 functionalized 30 nm AuNSs taken up by the HSC-3 cells was 10 times greater than those loaded on 15 nm AuNSs ($P < 0.05$). This supports similar findings reported by Jiang et al.,[15] which showed that the total number of ligands bound to the NP surface is directly related to the surface area of the nanoparticle The higher surface curvature of small NPs decreases the docking efficiency of the ligands by limiting their relative surface orientation. On the other hand, larger nanoparticles have a higher ligand-to-nanoparticle ratio, therefore increasing the drug loading capacity of the nanoparticle, allowing for active communication with the cell surface and subsequent receptor mediated endocytosis. As a result, larger nanoparticles will deliver more XAV939 into HSC-3 cells than the small ones, enhancing the required drug effect in terms of inducing G1 cell phase arrest. Additionally, coupling the higher drug loading capacity of the larger AuNSs with their enhanced receptor-mediated endocytosis consequently boosts the drug uptake by the cells and improves its selective cytotoxicity.

Similar reports state that nanoparticle cellular uptake, via receptor-mediated endocytosis, is greatly optimized when using nanoparticles between 30 and 50 nm in size.[47,48] One explanation could be that large nanoparticles have a larger contact area with the cell membrane receptors compared to

dx.doi.org/10.1021/bc400271x | Bioconjugate Chem. 2014, 25, 207−215

smaller ones, or because they hold more ligands/nanoparticle, enabling more interaction with the cell membrane. Therefore, one could state that the dynamics of functionalized nanoparticle HSC-3 cellular uptake greatly depend on the physical dimensions and surface chemistry.[49−55]

Cytotoxicity, Cell Cycle Analysis, and the Relative Uptake for the Free and Conjugated XAV939 Treated HaCaT Cells. The HaCaT cytotoxicity and cell cycle changes were closely monitored after being incubated with the same concentration of XAV939 used against HSC-3 cells for 48 and 96 h. Figure S2 illustrates the cytotoxicity of the HaCaT cells treated with free (a) and bioconjugated (b) forms of the drug at 48 and 96 h. HaCaT cellular viability decreased significantly after 96 h of treatment with free XAV (Figure S2a). On the other hand, nanoscaled XAV bioconjugates showed no significant cytotoxicity against HaCaT cells at both time points (Figure S2b). We then investigated the cell cycle changes associated with incubating the HaCat cells with free and conjugated forms of the XAV939 for 48 and 96 h. As shown in Figure S3, HaCaT cells treated with free and bioconjugated XAV939 showed no significant cell cycle change from the untreated cells (controls). Despite the selectivity of XAV939 toward HSC-3 cells, the effective lethal dose of the drug in its free form is considerably high (178 μM). As a result, when subjecting the HaCaT cells to such concentrations of the free form, adverse effects on their proliferation were still noticed. Loading the drug on 15 and 30 nm AuNSs significantly decreased the effective drug concentration by at least an order of magnitude. As a result, HaCaT cell death and any underlying cell phase changes were considerably minimized when compared to that caused by the free form of XAV939 (Figures S2 and S5).

The AuNS cellular localization and drug uptake were further investigated in the HaCaT cells. We compared the uptake values of XAV939 drug conjugates between the cancerous (HSC-3) and noncancerous (HaCaT) cell lines. The HaCaT cells exhibited a 6.6- and 7.5-fold decrease in 30 and 15 nm XAV-AuNSs uptake, respectively, compared to HSC-3 after 48 h (Figures 6 and S6, $P < 0.05$). At 96 h, both the 15 and 30 nm XAV939 conjugates showed a 3-fold decrease in HaCaT cellular uptake when compared to the HSC-3 cells at the same time point. This was achieved by targeting the HSC-3 cell $\alpha_v\beta_6$ surface integrins and tankyrase enzyme using RGD and XAV939 ligands, respectively. It is worth mentioning that there was an order of magnitude higher HaCaT cellular uptake for the larger functionalized AuNSs than the small ones. This can be further explained by the nonspecific enhanced receptor mediated endocytosis associated with the larger AuNSs.

Finally, dark field images of HaCaT cells incubated with 15 and 30 nm AuNSs showed minimal intracellular localization of both the drug loaded nanoparticles and the PEG stabilized ones (Figure S7).

CONCLUSION

To conclude, different-sized AuNSs were successfully conjugated and used as drug carriers for a novel inhibitor, XAV939, to actively interact and selectively target human oral squamous cell carcinoma. Cellular cytotoxicity, cell cycle distribution, and uptake data all demonstrated that the efficacy of XAV939 is significantly enhanced when presented as a gold nanoparticle bioconjugate compared to its free form. In addition, the cytotoxicity of XAV939 bioconjugates against HSC-3 cells was found to fairly compete with some of the popular HSC-3 anticancer drugs reported in the literature. We also defined the nanoparticle size range, drug concentration range, and treatment time as critical parameters that affect the drug delivery and efficacy. The drug efficacy dependence on nanoparticle size is attributed to receptor-mediated endocytosis and therefore the amount of drug internalized by the cell. A full understanding of the underlying mechanism has not yet been revealed; however, the augmented potency and selective intracellular delivery of XAV939 conjugates opens opportunities to further understanding the cellular interactions with such biosystems. Further studies are being conducted to investigate the intracellular interaction with the XAV939-conjugated nanoparticles.

ASSOCIATED CONTENT

Supporting Information

Drug dose-dependent graphs for HSC-3 cells incubated with both free and bioconjugated forms of XAV939 for 48 h, and cell viabilities of HSC-3 cells incubated with AuNSs conjugated with other ligands as control are included. Cell cycle analysis of HSC-3 cells after being incubated with both sizes of P-AuNSs, and PR AuNSs as controls. Additionally, drug-dose dependent graphs, cell cycle analysis, cellular uptake, and dark field images of HaCaT cells incubated with XAV939 bioconjugates. This material is available free of charge via the Internet at http://pubs.acs.org.

AUTHOR INFORMATION

Corresponding Author

*E-mail: melsayed@gatech.edu. phone: 404.894.0292. fax: 404.894.0294.

Present Address

Marwa M. Afifi, Department of Oral Pathology, Faculty of Dentistry, Alexandria University, Egypt.

Author Contributions

L.A.A. and M.A.M. contributed equally to this work.

Notes

The authors declare no competing financial interest.

ACKNOWLEDGMENTS

M.A.E. would like to thank Julius Brown Chair Funding (3306559GT) and the National Institutes of Health-National Cancer Institute grant U01CA151802.

REFERENCES

(1) Nie, S., Xing, Y., Kim, G. J., and Simons, J. W. (2007) Nanotechnology applications in cancer. *Annu. Rev. Biomed. Eng. 9*, 257−288.

(2) Ghosh, P., Han, G., De, M., Kim, C. K., and Rotello, V. M. (2008) Gold nanoparticles in delivery applications. *Adv. Drug Delivery Rev. 60*, 1307−1315.

(3) Panyala, N. R., Pena-Mendez, E., and Havel, J. (2009) Gold and nano-gold in medicine: overview, toxicology and perspectives. *J. Appl. Biomed. 7*, 75−91.

(4) Kim, B. Y. S., Rutka, J. T., and Chan, W. C. W. (2010) Current concepts: nanomedicine. *New. Engl. J. Med. 363*, 2434−2443.

(5) Prabhu, P., and Patravale, V. (2012) The upcoming field of theranostic nanomedicine: an overview. *J. Biomed. Nanotechnol. 8*, 859−82.

(6) Dreaden, E. C., Alkilany, A. M., Huang, X. H., Murphy, C. J., and El-Sayed, M. A. (2012) The golden age: gold nanoparticles for biomedicine. *Chem. Soc. Rev. 41*, 2740−2779.

(7) Alkilany, A. M., Lohse, S. E., and Murphy, C. J. (2013) The gold standard: gold nanoparticle libraries to understand the nano-bio interface. *Acc. Chem. Res. 46*, 650−661.
(8) Tiwari, P. M., Vig, K., Dennis, V. A., and Singh, S. R. (2011) Functionalized gold nanoparticles and their biomedical applications. *Nanomaterials 1*, 31−63.
(9) Aryal, S., Grailer, J. J., Pilla, S., Steeber, D. A., and Gong, S. Q. (2009) Doxorubicin conjugated gold nanoparticles as water-soluble and pH-responsive anticancer drug nanocarriers. *J. Mater. Chem. 19*, 7879−7884.
(10) Paciotti, G. F., Myer, L., Weinreich, D., Goia, D., Pavel, N., McLaughlin, R. E., and Tamarkin, L. (2004) Colloidal gold: a novel nanoparticle vector for tumor directed drug delivery. *Drug Delivery 11*, 169−183.
(11) Bhumkar, D. R., Joshi, H. M., Sastry, M., and Pokharkar, V. B. (2007) Chitosan reduced gold nanoparticles as novel carriers for transmucosal delivery of insulin. *Pharm. Res. 24*, 1415−1426.
(12) Dreaden, E. C., Mwakwari, S. C., Sodji, Q. H., Oyelere, A. K., and El-Sayed, M. A. (2009) Tamoxifen-poly(ethylene glycol)-thiol gold nanoparticle conjugates: enhanced potency and selective delivery for breast cancer treatment. *Bioconjugate Chem. 20*, 2247−2253.
(13) Dong, X. W., and Mumper, R. J. (2010) Nanomedicinal strategies to treat multidrug-resistant tumors: current progress. *Nanomedicine (London, U.K.) 5*, 597−615.
(14) Oyelere, A. K., Chen, P. C., Huang, X. H., El-Sayed, I. H., and El-Sayed, M. A. (2007) Peptide-conjugated gold nanorods for nuclear targeting. *Bioconjugate Chem. 18*, 1490−1497.
(15) Jiang, W., Kim, B. Y. S., Rutka, J. T., and Chan, W. C. W. (2008) Nanoparticle-mediated cellular response is size-dependent. *Nat. Nanotechnol. 3*, 145−150.
(16) Reverter, J. (2009) Gold nanoparticles as carriers of cisplatin with a pH sensitive linker for intracellular drug delivery. *New Biotechnol. 25*, S39−S39.
(17) Roa, W., Zhang, X., Guo, L., Shaw, A., Hu, X., Xiong, Y., Gulavita, S., Patel, S., Sun, X., Chen, J., Moore, R., and Xing, J. Z. (2009) Gold nanoparticle sensitize radiotherapy of prostate cancer cells by regulation of the cell cycle. *Nanotechnology 20*, 37.
(18) Wang, Y. L., Chen, J. J., and Irudayaraj, J. (2011) Nuclear targeting dynamics of gold nanoclusters for enhanced therapy of HER2(+) breast cancer. *ACS Nano 5*, 9718−9725.
(19) Huang, X. H., El-Sayed, I. H., Qian, W., and El-Sayed, M. A. (2006) Cancer cell imaging and photothermal therapy in the near-infrared region by using gold nanorods. *J. Am. Chem. Soc. 128*, 2115−2120.
(20) Dellinger, T. H., Planutis, K., Tewari, K. S., and Holcombe, R. F. (2012) Role of canonical Wnt signaling in endometrial carcinogenesis. *Expert Rev. Anticancer Ther. 12*, 51−62.
(21) Zhang, M. F., Shi, J. P., Huang, Y. D. and Lai, L. J. (2012) Expression of canonical WNT/beta-CATENIN signaling components in the developing human lung. *BMC Dev. Biol. 12*.
(22) Kypta, R. M., and Waxman, J. (2012) Wnt/beta-catenin signalling in prostate cancer. *Nat. Rev. Urol. 9*, 418−428.
(23) MacDonald, B. T., Tamai, K., and He, X. (2009) Wnt/beta-catenin signaling: components, mechanisms, and diseases. *Dev. Cell 17*, 9−26.
(24) Rhee, C. S., Sen, M., Lu, D. S., Wu, C., Leoni, L., Rubin, J., Corr, M., and Carson, D. A. (2002) Wnt and frizzled receptors as potential targets for immunotherapy in head and neck squamous cell carcinomas. *Oncogene 21*, 6598−6605.
(25) Uraguchi, M., Morikawa, M., Shirakawa, M., Sanada, K., and Imai, K. (2004) Activation of WNT family expression and signaling in squamous cell carcinomas of the oral cavity. *J. Dent. Res. 83*, 327−332.
(26) Clevers, H. (2006) Wnt/beta-catenin signaling in development and disease. *Cell 127*, 469−480.
(27) Verkaar, F., and Zaman, G. J. R. (2011) New avenues to target Wnt/beta-catenin signaling. *Drug Discovery Today 16*, 35−41.
(28) Huang, S. M., Mishina, Y. M., Liu, S., Cheung, A., Stegmeier, F., Michaud, G. A., Charlat, O., Wiellette, E., Zhang, Y., Wiessner, S., Hild, M., Shi, X., Wilson, C. J., Mickanin, C., Myer, V., Fazal, A., Tomlinson, R., Serluca, F., Shao, W., Cheng, H., Shultz, M., Rau, C., Schirle, M., Schlegl, J., Ghidelli, S., Fawell, S., Lu, C., Curtis, D., Kirschner, M. W., Lengauer, C., Finan, P. M., Tallarico, J. A., Bouwmeester, T., Porter, J. A., Bauer, A., and Cong, F. (2009) Tankyrase inhibition stabilizes axin and antagonizes Wnt signalling. *Nature 461*, 614−620.
(29) Chen, B., Dodge, M. E., Tang, W., Lu, J., Ma, Z., Fan, C. W., Wei, S., Hao, W., Kilgore, J., Williams, N. S., Roth, M. G., Amatruda, J. F., Chen, C., and Lum, L. (2009) Small molecule-mediated disruption of Wnt-dependent signaling in tissue regeneration and cancer. *Nat. Chem. Biol. 5*, 100−107.
(30) Noguti, J., De Moura, C. F. G., Hossaka, T. A., Franco, M., Oshima, C. T. F., Dedivitis, R. A., and Ribeiro, D. A. (2012) The role of canonical WNT signaling pathway in oral carcinogenesis: a comprehensive review. *Anticancer Res. 32*, 873−878.
(31) Priyadarsini, R. V., Murugan, R. S., and Nagini, S. (2012) Aberrant activation of Wnt/beta-catenin signaling pathway contributes to the sequential progression of DMBA-induced HBP carcinomas. *Oral Oncol. 48*, 33−39.
(32) Frens, G. (1973) Controlled nucleation for the regulation of the particle size in monodisperse gold suspensions. *Nat. Phys. Sci. 241*, 20.
(33) Austin, L. A., Kang, B., Yen, C. W., and El-Sayed, M. A. (2011) Nuclear targeted silver nanospheres perturb the cancer cell cycle differently than those of nanogold. *Bioconjugate Chem. 22*, 2324−2331.
(34) Ulman, A. (1996) Formation and structure of self-assembled monolayers. *Chem. Rev. 96*, 1533−1554.
(35) Xue, H. A., Zhu, W., Li, X., Ramos, D. M., and Pytela, R. (2004) Role of the $\alpha v\beta 6$ integrin in human oral squamous cell carcinoma growth in vivo and in vitro. *Biochem. Biophys. Res. Commun. 288*, 610−618.
(36) Chen, X. Y., Plasencia, C., Hou, Y. P., and Neamati, N. (2005) Synthesis and biological evaluation of dimeric RGD peptide-paclitaxel conjugate as a model for integrin-targeted drug delivery (vol 48, pg 1099, 2005). *J. Med. Chem. 48*, 5874−5874.
(37) Tarazona-Vasquez, F., and Balbuena, P. B. (2004) Complexation of the lowest generation poly(amidoamine)-NH2 dendrimers with metal ions, metal atoms, and Cu((II)) hydrates: An ab initio study. *J. Phys. Chem. B 108*, 15992−16001.
(38) Vilan, A., Ussyshkin, R., Gartsman, K., Cahen, D., Naaman, R., and Shanzer, A. (1998) Real-time electronic monitoring of adsorption kinetics: Evidence for two-site adsorption mechanism of dicarboxylic acids on GaAs(100). *J. Phys. Chem. B 102*, 3307−3309.
(39) Levy, R., Thanh, N. T. K., Doty, R. C., Hussain, I., Nichols, R. J., Schiffrin, D. J., Brust, M., and Fernig, D. G. (2004) Rational and combinatorial design of peptide capping Ligands for gold nanoparticles. *J. Am. Chem. Soc. 126*, 10076−10084.
(40) Zhang, Z. P., and Feng, S. S. (2006) The drug encapsulation efficiency, in vitro drug release, cellular uptake and cytotoxicity of paclitaxel-loaded poly(lactide)-tocopheryl polyethylene glycol succinate nanoparticles. *Biomaterials 27*, 4025−4033.
(41) Bandyopadhyay, A., and Raghavan, S. (2009) Defining the role of integrin alphavbeta6 in cancer. *Curr. Drug Targets 10*, 645−652.
(42) Cho, E. C., Au, L., Zhang, Q., and Xia, Y. N. (2010) The effects of size, shape, and surface functional group of gold nanostructures on their adsorption and internalization by cells. *Small 6*, 517−522.
(43) Massague, J. (2004) G1 cell-cycle control and cancer. *Nature 432*, 298−306.
(44) Michalides, R. J., van de Brekel, M., and Balm, F. (2002) Defects in G1-S cell cycle control in head and neck cancer: a review. *Head & Neck 24*, 694−704.
(45) Jain, P. K., Huang, X. H., El-Sayed, I. H., and El-Sayed, M. A. (2008) Noble metals on the nanoscale: optical and photothermal properties and some applications in imaging, sensing, biology, and medicine. *Acc. Chem. Res. 41*, 1578−1586.
(46) Kang, B., Mackey, M. A., and El-Sayed, M. A. (2010) Nuclear targeting of gold nanoparticles in cancer cells induces DNA damage, causing cytokinesis arrest and apoptosis. *J. Am. Chem. Soc. 132*, 1517−+.
(47) Osaki, F., Kanamori, T., Sando, S., Sera, T., and Aoyama, Y. (2004) A quantum dot conjugated sugar ball and its cellular uptake on

the size effects of endocytosis in the subviral region. *J. Am. Chem. Soc. 126*, 6520−6521.
(48) Chithrani, B. D., Ghazani, A. A., and Chan, W. C. W. (2006) Determining the size and shape dependence of gold nanoparticle uptake into mammalian cells. *Nano Lett. 6*, 662−668.
(49) Elbakry, A., Wurster, E. C., Zaky, A., Liebl, R., Schindler, E., Bauer-Kreisel, P., Blunk, T., Rachel, R., Goepferich, A., and Breunig, M. (2012) Layer-by-layer coated gold nanoparticles: size-dependent delivery of DNA into cells. *Small 8*, 3847−3856.
(50) Badwaik, V. D., Vangala, L. M., Pender, D. S., Willis, C. B., Aguilar, Z. P., Gonzalez, M. S., Paripelly, R. and Dakshinamurthy, R. (2012) Size-dependent antimicrobial properties of sugar-encapsulated gold nanoparticles synthesized by a green method. *Nanoscale Res. Lett. 7*.
(51) Etame, A. B., Smith, C. A., Chan, W. C. W., and Rutka, J. T. (2011) Design and potential application of PEGylated gold nanoparticles with size-dependent permeation through brain microvasculature. *Nanomed. Nanotechnol. 7*, 992−1000.
(52) Cebrian, V., Martin-Saavedra, F., Yague, C., Arruebo, M., Santamaria, J., and Vilaboa, N. (2011) Size-dependent transfection efficiency of PEI-coated gold nanoparticles. *Acta Biomater. 7*, 3645−3655.
(53) Zhang, X. D., Wu, D., Shen, X., Liu, P. X., Yang, N., Zhao, B., Zhang, H., Sun, Y. M., Zhang, L. A., and Fan, F. Y. (2011) Size-dependent in vivo toxicity of PEG-coated gold nanoparticles. *Int. J. Nanomed. 6*, 2071−2081.
(54) Gonzalez, M. G., Liu, X. J., Niessner, R., and Haisch, C. (2010) Strong size-dependent photoacoustic effect on gold nanoparticles by laser-induced nanobubbles. *Appl. Phys. Lett.*, 96.
(55) Pan, Y., Neuss, S., Leifert, A., Fischler, M., Wen, F., Simon, U., Schmid, G., Brandau, W., and Jahnen-Dechent, W. (2007) Size-dependent cytotoxicity of gold nanoparticles. *Small 3*, 1941−1949.
(56) Austin, L. A., Kang, B., and El-Sayed, M. A. (2013) A new nanotechnology technique for determining drug efficacy using targeted plasmonically enhanced single cell imaging spectroscopy. *J. Am. Chem. Soc. 135*, 4688−4691.
(57) Suzuki, F., Hashimoto, K., Kikuchi, H., Nishikawa, H., Matsumoto, H., Shimada, J., Kawase, M., Sunaga, K., Tsuda, T., Satoh, K., and Sakagami, H. (2005) Induction of tumor-specific cytotoxicity and apoptosis by doxorubicin. *Anticancer Res. 25*, 887−893.
(58) Park, J. Y., Kang, J. H., Yun, P. Y., Myoung, H., Lee, J. H., and Kim, M. J. (2007) The role of tamoxifen in combination with cisplatin on oral squamous cell carcinoma cell lines. *Oral Oncol.*, 118−118.